Electrical Power and Energy Systems 154 (2023) 109426

Contents lists available at ScienceDirect

International Journal of Electrical Power and Energy Systems

journal homepage: www.elsevier.com/locate/ijepes

Upper bound of overvoltage peak induced in power line network above lossless ground due to radiated electromagnetic disturbances

Tao Liang [a,b,*], Giordano Spadacini [c], Sergio A. Pignari [c], Yan-zhao Xie [a,b]

[a] State Key Laboratory of Electrical Insulation and Power Equipment, Xi'an Jiaotong University, No. 28, Xianning West Road, Xi'an 710049, China
[b] School of Electrical Engineering, Xi'an Jiaotong University, No. 28, Xianning West Road, Xi'an 710049, China
[c] Dipartimento di Elettronica, Informazione e Bioingegneria (DEIB), Politecnico di Milano, Piazza Leonardo da Vinci, 32, Milan 20134, Italy

ARTICLE INFO

Keywords:
Power line network
Worst-case scenario
Overvoltage
Radiated electromagnetic disturbance
Transmission line model

ABSTRACT

This paper deals with the assessment of the maximal peak of the overvoltage induced in a power-line network due to the field-to-wire coupling from an external electromagnetic disturbance. A worst-case analysis is here combined with the transmission line model to find the terminal overvoltage, induce by radiated electromagnetic disturbances of constrained energy density and bandlimits. The approach was applied to canonic power line network topologies, from statistic viewpoint, it is demonstrated that dominant coupling can be ascribed to the branch containing the most twisted segments. Accordingly, efforts have been devoted to find analytical solution to overvoltage peak upper bound for the coupling-dominant zigzag branch. In this connection, both versatile implicit solution and approximated explicit expressions of the upper bound are formulated, which reveals the relations between the upper bound of zigzag branch and its segments, quantitively interpreting the effect of segment orientations and length. Finally, numerical simulations corroborate the model validity and suggest that the estimations of upper bound are sufficiently accurate for analyzing practical power line network. This proposed approach will be instructive for power system insulation coordination and protection design.

1. Introductions

Overvoltage in power lines induced by external electromagnetic fields poses a serious threat on safety operation of the primary and secondary power equipment [1,2]. Similar to transient overvoltage disturbed by direct lightning strikes and very fast transient overvoltage (VFTO), which has been widely studied in terms of model strategies [3], measurement techniques [4–6] and protection methods [7], overvoltage induced by external field coupling to the power lines has also received extensive attentions, since the potential damages caused by external field radiation on power systems and connected equipment cannot be overlooked, [8–14]. To name a few relevant studies: indirect lightning strikes (lightning hits ground in proximity of the power line) could induce overvoltage surges on power lines and lead to flashover of line insulators [13–17]. Geomagnetic disturbances (GMD) caused by solar flares may be responsible for low-frequency current injection into power lines, resulting in saturation of transformers cores and power system instability [18–20]. High-altitude electromagnetic pulses can induce fast-rising, double-exponential shaped waveforms in wide-range power systems, causing damage to equipment (e.g., transformer, potential/current transformer, etc.) [21,22]. Recent years have witnessed growing interests in assessing the threats of radiated electromagnetic disturbances to complex power systems, including identifying sources of possibly hazardous fields, modelling and predicting damaging effects on equipment and system levels, etc. [2,23,24].

However, due to the wide variability of the distinctive features of the external electromagnetic disturbances and the complexity of the coupling phenomenon, quantitative assessment of the induced overvoltage remains a challenging task, it should be noted that, besides indirect lightning, GMD and HEMP mentioned above, the incessant evolution of electrical and electronic technologies continues to increase the possibly hazardous electromagnetic disturbances. Accordingly, the impinging field may be characterized by distinct time-domain waveforms (double-exponential pulses, damped sinusoids, Gaussian pulses, etc.) with narrow- or wide-band frequency spectra. However, a survey of a limited number of electromagnetic field waveforms in a specific system presents a very one-sided picture of the conclusions. On the other hand, it is of great interest to approach the problem in a reversed

* Corresponding author.
E-mail addresses: tao.liang@xjtu.edu.cn (T. Liang), giordano.spadacini@polimi.it (G. Spadacini), sergio.pignari@polimi.it (S.A. Pignari), yzxie@xjtu.edu.cn (Y.-z. Xie).

https://doi.org/10.1016/j.ijepes.2023.109426
Received 17 March 2023; Received in revised form 4 July 2023; Accepted 4 August 2023
Available online 10 August 2023

fashion. Instead of accurate predicting field induced power system overvoltage from individual external disturbances of distinct waveform characteristics, consider the worst-case scenario by assessing the upper bound of overvoltage peak that could be possibly induced due to radiated fields of arbitrary waveform. This analysis can be informative for power system insulation coordination and protection design.

In this regard, a series of investigations have been carried out recently. In [25,26], by assuming the external field carrying a bounded bandwidth and finite energy density, the worst-case field waveform which maximizes the peak of the induced-voltage waveform was obtained for a general victim system. This worst-case model was later reformulated in [27] for a straight wire running parallel above ground using transmission-line (TL) theory. In addition to the improved computational efficiency, TL formulation of the field-to-wire coupling problem enabled deriving closed-form expressions, unveiling the impacts of parameters like length, height, and terminal loads on the induced worst-case voltage peak.

The worst-case analysis method can be exploited to predict the upper bound of field-induced overvoltage for simple straight line. However, it is still a challenging task to make predictions for real-world power lines system, which usually has complex routing paths to accommodate environmental constraints as well as urban layouts. In this regard, this paper extends the worst-case analysis method to power line system of complex routing topology. The main objective is the identification of dominant coupling path and the derivation of analytical expressions of overvoltage upper bound, pointing out the contribution of different straight segments in the whole network and revealing the impact of different routing topology.

The following hypothesis are adopted as necessary steps for simplifying the problem:

- Since the overvoltage due to field coupling to power line is dominated by common mode coupling, the practical multiconductor TLs (3-phase conductors, shielding line, etc.) are equivalently represented by single conductor TL.
- A wide-range external electromagnetic field excites the entire power line network simultaneously. To avoid overestimation, TL network under analysis is limited to the parts where physical illumination by external disturbances occurs.
- Both conductors and ground are assumed to be lossless for simplicity. Power line network is composed of straight-line segments and terminal lumped loads (modelling equipment like transformers, etc.), without losing generality, the terminal overvoltage associated to equipment at origin of the coordinates is assumed to be target of the analysis.

The paper is organized as follows: Section 2 summarizes the key steps to evaluate the field coupling efficiency of the power line network with TL theory. Section 3 presents the prediction theory for overvoltage peak upper bound in power line systems, the impacts of topology on the statistics of overvoltage peak are investigated via numerical examples, both the implicit and explicit expressions to the upper bound of the field-induced overvoltage peak are formulated for the coupling-dominated branch. Section 4 validates the proposed method through case study. Finally, Section 5 draws the final conclusions. In addition, a step-by-step derivation of the implicit expression for upper bound prediction is reported in Appendix A.

2. Generic approach for assessing upper bound of field induced overvoltage on power-line network

2.1. Power-line network under study and deterministic field-coupling efficiency estimation

A generalized representation of complex power-line system is shown in Fig. 1. All segments are assumed to be made of a lossless conductor of radius r_w, and running at height h above a lossless ground. The power line network follows complex routing to accommodate to the landscape and urban planning. The terminal of power line is connected to power equipment, which can be modelled by lumped circuit according to the

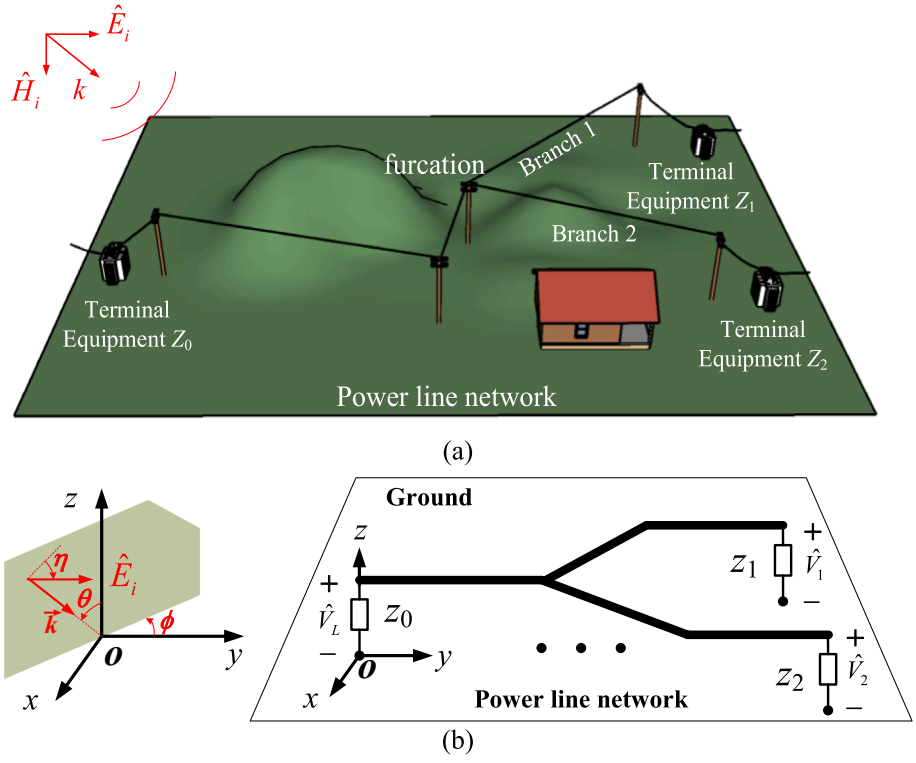

Fig. 1. (a) Generic representation of power-line network excited by an external electromagnetic field, complex routing is adopted to accommodate the landscape; (b) Simplified illustration of power line network model (right) and definition of incidence θ, ϕ and polarization angle η of incident field (left).

frequency range of impinging field. Without losing generality, assuming the overvoltage at one of the terminal transformers is of concern, imposing the origin of coordinates at this point. Modelling the external impinging field as a linearly polarized plane wave with propagation vector $\overrightarrow{k}$ and incident electrical field $\overrightarrow{\widehat{E}}^{\mathrm{inc}}$. The incidence direction is defined in spherical coordinates by the polar angle θ and the azimuth angle ϕ, while the polarization is defined by the angle η between the electric-field vector and the incidence plane. As a result, the electrical field $\widehat{E}_i$ can be decomposed as orthogonal components $\widehat{E}_x^{\mathrm{inc}}$, $\widehat{E}_y^{\mathrm{inc}}$ and $\widehat{E}_z^{\mathrm{inc}}$ aligning to the direction vector $\overrightarrow{u}_x$, $\overrightarrow{u}_y$ and $\overrightarrow{u}_z$ of *x*-, *y*-, *z*-axis, respectively, that is,

$$\begin{aligned}\overrightarrow{\widehat{E}}^{\mathrm{inc}}(x,y,z) &= \left(\widehat{E}_x^{\mathrm{inc}}\overrightarrow{u}_x + \widehat{E}_y^{\mathrm{inc}}\overrightarrow{u}_y + \widehat{E}_z^{\mathrm{inc}}\overrightarrow{u}_z\right)e^{-\mathrm{j}\left(k_x x+k_y y+k_z z\right)}\\ \widehat{E}_x^{\mathrm{inc}} &= \widehat{E}_i(-\cos\theta\sin\phi\cos\eta+\cos\phi\sin\eta)\\ \widehat{E}_y^{\mathrm{inc}} &= \widehat{E}_i(\cos\theta\cos\phi\cos\eta+\sin\phi\sin\eta)\\ \widehat{E}_z^{\mathrm{inc}} &= \widehat{E}_i\sin\theta\cos\eta\end{aligned} \tag{1}$$

Due to reflection from ground, the total electrical field $\overrightarrow{\widehat{E}}^{tot}$ above ground is the superposition of incident field and reflection field, i.e., $\overrightarrow{\widehat{E}}^{tot} = \overrightarrow{\widehat{E}}^{inc} + \overrightarrow{\widehat{E}}^{ref}$, with

$$\overrightarrow{\widehat{E}}^{\mathrm{ref}}(x,y,z) = \left(-\widehat{E}_x^{\mathrm{inc}}\overrightarrow{u}_x - \widehat{E}_y^{\mathrm{inc}}\overrightarrow{u}_y + \widehat{E}_z^{\mathrm{inc}}\overrightarrow{u}_z\right)e^{-\mathrm{j}\left(k_x x+k_y y-k_z z\right)} \tag{2}$$

Where j is the imaginary unit, propagation constant components are given by: $k_x = -k\sin\theta\sin\phi$, $k_y = k\sin\theta\cos\phi$, $k_z = -k\cos\theta$, wave number $k = 2\pi f/c_0$, f is frequency of the impinging field.

Without losing generality, considering a TL network composed by n line segment of length [l_0, l_1, …], height h and radius r_w, let the voltage across load Z_0 being the interest of evaluation ($\widehat{V}_L$). Resorting to the Baum-Liu-Tesche (BLT) modelling approach, the field-induced voltage across all terminal load ($\boldsymbol{V_L} = [\widehat{V}_L,\ \widehat{V}_1, \cdots]^{\mathrm{T}}$)in the frequency domain can be solved by, [28,29]:

$$\boldsymbol{V_L} = (\boldsymbol{U}+\boldsymbol{\rho})(-\boldsymbol{\rho}+\boldsymbol{\Gamma})^{-1}\boldsymbol{S}; \tag{3}$$

Where $\boldsymbol{U}$ is an identity matrix. Voltage reflection coefficient $\boldsymbol{\rho}$ is a diagonal matrix, whose i^{th} diagonal element is given by $\rho_{ii} = (Z_i - Z_{Ci})(Z_i + Z_{Ci})^{-1}$, Z_{Ci} is the characteristic impedance of line, [30]. Propagation matrix $\boldsymbol{\Gamma}$ is cast as

$$\boldsymbol{\Gamma} = \begin{bmatrix}\boldsymbol{0} & \boldsymbol{P}\\ \boldsymbol{P} & \boldsymbol{0}\end{bmatrix}, \tag{4}$$

Where $\boldsymbol{0}$ is n-by-n zeros, $\boldsymbol{P}$ summarizes the propagation term $\mathrm{e}^{\mathrm{j}kl_i}$ associated to i^{th} segment of line length l_i. The source matrix $\boldsymbol{S} = [\boldsymbol{S_1}, \boldsymbol{S_2}]^{\mathrm{T}}$ represents the equivalent source due to external field illumination, [31]. Accordingly, for the i^{th} line segment connecting terminal $\left(x_i^L, y_i^L, z_i^L\right)$ and terminal at $\left(x_i^R, y_i^R, z_i^R\right)$, source term can be evaluated as:

$$S_1 = \frac{1}{2}\int_0^{l_i}\mathrm{e}^{\mathrm{j}k\tau}\widehat{V}_{\mathrm{S}}(\tau)\mathrm{d}\tau + \frac{\widehat{V}_{\mathrm{SL}}}{2} - \frac{\widehat{V}_{\mathrm{SR}}}{2}\mathrm{e}^{\mathrm{j}kl_i} \tag{5}$$

$$S_2 = -\frac{1}{2}\int_0^{l_i}\mathrm{e}^{\mathrm{j}k(l_i-\tau)}\widehat{V}_{\mathrm{S}}(\tau)\mathrm{d}\tau - \frac{\widehat{V}_{\mathrm{SL}}}{2}\mathrm{e}^{\mathrm{j}kl_i} + \frac{\widehat{V}_{\mathrm{SR}}}{2} \tag{6}$$

In which, $\widehat{V}_S = \widehat{E}^{tot}(x,y,h)\cdot\overrightarrow{u}_{l_i} - \widehat{E}^{tot}(x,y,0)\cdot\overrightarrow{u}_{l_i}$ represents the contribution due to the tangential electrical field component along the line, $\overrightarrow{u}_{l_i}$ is direction vector along the i^{th} line segment. Whereas, the vertical field component leads to:

$$\begin{aligned}\widehat{V}_{SL} &= \int_0^h \overrightarrow{E}^{\mathrm{tot}}\left(x_i^L, y_i^L, z\right)\cdot\overrightarrow{u}_z dz;\\ \widehat{V}_{SR} &= \int_0^h \overrightarrow{E}^{\mathrm{tot}}\left(x_i^R, y_i^R, z\right)\cdot\overrightarrow{u}_z dz;\end{aligned} \tag{7}$$

Combing (1)-(7), the terminal voltage of interest $\widehat{V}_L$ could finally been solved. For convenience, defining the *coupling efficiency* as $\widehat{L} = \widehat{V}_L/\widehat{E}_i$, namely, the transfer ratio between the induced overvoltage and the impinging electric field intensity. It is worth noting that, although perfect ground has been assumed for the formulation of BLT approach, the effect of lossy ground could also be incorporated by resorting to Sunde's approximation for assessing ground impedance, [10,29] and Cooray-Rubinstein's formula for quantifying reflection of incident field, [10,32]. In this connection, the following worst-case analysis could be smoothly applied to numerically predict the overvoltage upper bound.

2.2. Worst-case analysis method and upper bound of overvoltage peak estimation approach

With knowledge of *coupling efficiency* $\widehat{L}$ for given power line network, let us consider an impinging electromagnetic field with limited frequency bandwidth [f_1, f_2] and finite energy density W_{E} (unit: J/m^2). Such assumptions originate from physical limitations of practical pulsed electromagnetic field [25]. Accordingly, resorting to the worst-case analysis approach, the maximal peak of overvoltage waveform propagating the network could be identified by solving the optimization problem:

$$\begin{aligned}\max:\quad & V_P = \frac{1}{2\pi}\int_{-\infty}^{+\infty}\widehat{E}_i\cdot\widehat{L}e^{j\omega t_0}d\omega\\ s.t.:\quad & \frac{1}{2\pi Z_0}\int_{-\infty}^{+\infty}|\widehat{E}_i(\omega)|^2 d\omega = W_E\end{aligned} \tag{8}$$

where $Z_0 \approx 377\ \Omega$ is the free-space wave impedance. Through a rigorous functional analysis, it was demonstrated in [27] that the upper bound of the overvoltage peak is

$$V_P = \sqrt{\frac{Z_0 W_E}{\pi}\int_{\omega_1}^{\omega_2}|\widehat{L}|^2 d\omega} \tag{9}$$

where $\omega_1 = 2\pi f_1$, $\omega_2 = 2\pi f_2$. the spectrum of the optimized external field waveform leading to expression:

$$\widehat{E}_i(\omega) = \sqrt{\frac{Z_0\pi W_E}{\int_{\omega_1}^{\omega_2}|\widehat{L}|^2 d\omega}}\widehat{L}^* e^{-j\omega t_0} \tag{10}$$

where t_0 is the time instant when the induced waveform reaches its peak.

To this end, by combining the worst-case approach and BLT model, one can estimate the upper bound of field induced overvoltage peak for arbitrary (topology, terminal equipment) power system and arbitrary (bandwidth, incidence, polarization, etc.) external disturbance. Note that this method also demonstrating wide practicability, solution to the upper bound of overvoltage peak (9) appears to be function of coupling efficiency $\widehat{L}$ only, it is convenient to apply other field-coupling model approach to deal with more complex power line networks, e.g., nonuniform TL model for including the impact of line sag. This paper resorts to BLT approach for modelling the power line network, which is a proper compromise between preciseness and efficiency.

3. Upper bound of overvoltage peak for complex power-line network

3.1. Power line network reduction in terms of statistics of overvoltage peak

In this section, we apply the proposed approach to canonical power networks to unveil the impact of different network topology, to simplify the system from the worst-case viewpoint.

Considering canonical TL parameters of a 10 kV distributed power line system, let wire radius $r_w = 13$ mm (overhead line model: JKLYJ/Q-10); height $h = 10$ m. According to this geometry, the per-unit-length parameters of the power line lead to characteristic impedance of $Z_C = 440\ \Omega$ [33]. In view of practical impinging field parameters, assuming the external field is constrained by limited bandwidth [1 Hz ~ 10 MHz] and energy density $W_E \leq 1$ mJ/m^2. Note that the energy density bound is selected based on statistics from a wide-range of practical electromagnetic radiators, [34], and also from indirect lightning field observations, [35], the value should be adjusted to accommodate less/more severe scenarios according to particular applications. In the following, we investigate the impacts of system parameters by case studies. The topology of TL network under consideration is defined by line segment length and orientation angle γ (with respect of $+y$ direction).

Since in general there is a lack of knowledge on the incidence and polarization of impinging field, Monte-Carlo (MC) statistical analysis is applied to estimate the statistical distribution of overvoltage peak upper bound. It is assumed the probability of incidences are equal for all directions, accordingly, the incidence angle (θ and ϕ) and polarization angle (η) are treated as random variables governed by distribution:

$$\theta = \text{acos}(1-2u); \qquad \phi = 2\pi v; \qquad \eta \sim \text{U}[0,\ 2\pi]; \tag{11}$$

Where axillary random variables follow uniform distributions: $u \sim \text{U}[0,1]$; $v \sim \text{U}[0,1]$. From a statistic viewpoint, the empirical cumulative distribution function (cdf) of overvoltage peak predicted by MC simulation could be used as figure-of-merit to quantify the worst-case field-coupling to power line system. Therefore, we analyze the impact of network topology by comparing cdfs.

3.1.1. Impact of line segment

The independence of upper bound of field induced overvoltage peak with respect to the length of segment is justified numerically through case studies in this section.

Firstly, a 1-branch TL network of 3-segment is considered, we control the orientation of line segment and change the length of line segments. MC method is resorted to evaluate the empirical cdf of predicted overvoltage with input random variables defined in (11). MC method is resorted to evaluate the empirical cdf of predicted overvoltage with input random variables defined in (11). Fig. 2 compares the predicted cdfs of V_P for different sampling size, the overlapped curves indicate all simulations have converged to the same results. As a result, 2000 samples, as a suitable trade-off between computational efficiency and preciseness, have been applied to the following MC simulations.

The obtained cdfs are summarized in Fig. 3, apparently, regardless the lengths, the cdfs are practically overlapping with each other. The result implies that maximal overvoltage is independent from the length of any segments.

In the second example, we increase the number of line segment to 5, in the same fashion, cdfs of the upper bound of overvoltage peak are evaluated and depicted in Fig. 4.

In the third example, we consider the extension of findings to branched TL network. Namely, 5-segment, 2-branch TL #7-#9 are considered for comparison, the rotation angles of all TLs are identical, where only the length of individual segments are changed. The results depicted in Fig. 5 further proving the independent of V_P distribution with respect to the segment length, since the cdfs are practically overlapping with each other, the impact of differences of segment lengths are

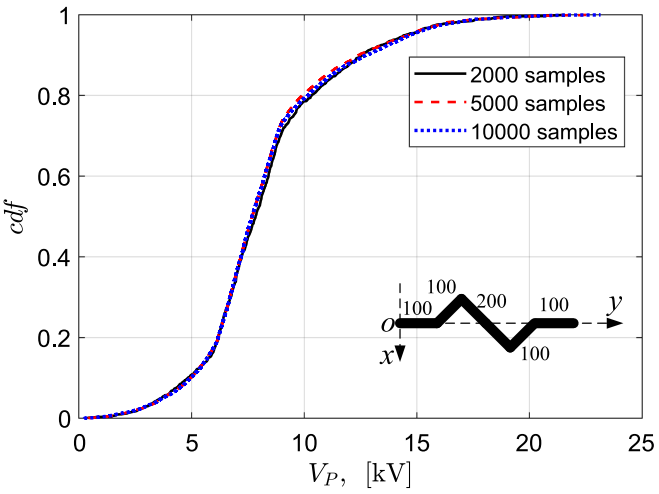

Fig. 2. Predicted empirical Cdfs of V_P for TL #4 with different random sampling size. Top view of TL layout is depicted in the inset, $Z_0 = 50\ \Omega$, $Z_1 = 300\ \Omega$.

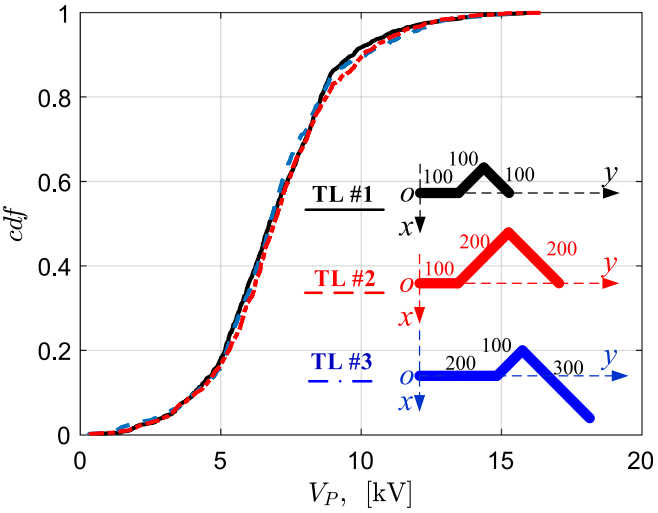

Fig. 3. Cdfs of VP for power-line network with changing line segment length. From left to right, rotation angles are: 0°, 45°, −45°, respectively. Line segment lengths are lists in the inset. General mismatched terminal impedances are assumed: $Z_0 = 50\ \Omega$, $Z_1 = 300\ \Omega$.

negligible.

It is also interesting to directly compare the results in Fig. 3 and Fig. 4. It appears that with two more segments, the predicted cdfs in Fig. 8 spread in a wider range from 0 V to around 23.2 kV, whereas the cdfs for a three-segment TL network range from 0 V to around 16.4 kV. Also, for the 0.8-quantile, the five-segment network foresees 10.5 kV, which is also larger than 8.8 kV for the three-segment network. This result suggests that worst-case external field coupling scenario will deteriorate when the power-line network contains more segments.

Conversely, by including Fig. 5 in the comparison, it is shown that even with same number of segments, the additional branch appear to reduce the predicted overvoltage peak (span narrower range in cdf), interesting still, cdf in Fig. 5 is much similar to Fig. 3, implying the contributions to V_P are determined by one branch only, while the other branch could be overlooked from the statistical viewpoint. This characteristic is of great interest from network reduction viewpoint, the conclusion will be further verified in following sections.

3.1.2. Impact of line segment orientation

In this section, we change the orientation of segment to investigate

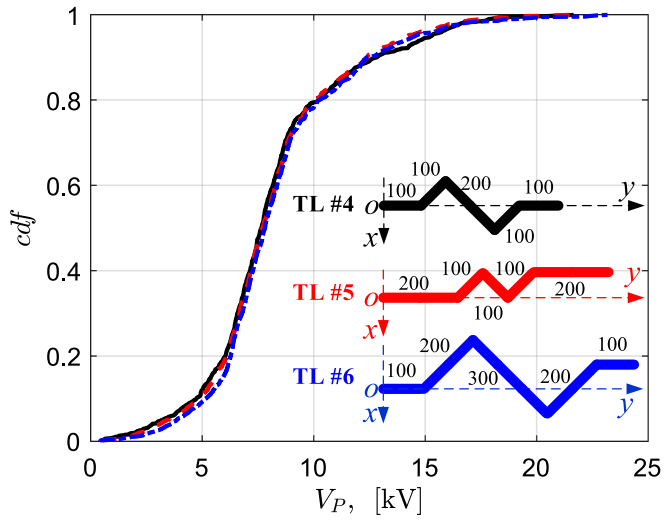

Fig. 4. Cdfs of V_P for power-line network with changing segment length. From left to right, rotation angles are: 0°, 45°, −45°, 45°, 0°, respectively. Line segment length are lists in the inset. $Z_0 = 50\ \Omega$, $Z_1 = 300\ \Omega$.

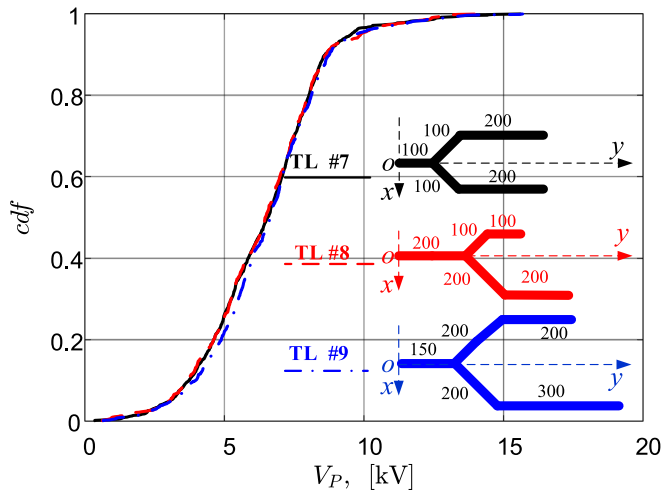

Fig. 5. Cdfs of V_P for power-line network with changing segment length. Line segment length are lists in the inset. $Z_0 = 50\ \Omega$, upper branch: terminal $Z_1 = 1$ kΩ, rotation angel 45°, 0°, lower branch: terminal $Z_2 = 300\ \Omega$, rotation angel −45°, 0°.

the impact on overvoltage peak. Firstly, considering a simple 2-segment line composed by two cascaded line of 100 m, the rotation angle of 2nd segment varies from 0° to 90°, the cdf of V_P is predicted and summarized in Fig. 6. In contrast to the length, the orientation angles of segments play a non-negligible role in overvoltage peak, with orientation angle increase, there is a clear wider spread of cdf, which suggests the overvoltage peak could be enlarged with drastic direction change.

3.1.3. Impact of cascaded segment number

The impact of cascaded segments is studied in this section, in Fig. 7, the cdf of a zigzag line composing 2 ∼ 5 segments are reported. It is evident that with cascaded segment number increasing, cdf spans in a wider range, the worst-case field coupling scenario is deteriorated. Therefore, from a statistical viewpoint, introducing less segments to the layout design can reduce the overvoltage level and ease the overvoltage stress on terminals.

3.1.4. Impact of branching

To analyze the impact of branching, we consider a zigzag TL #15

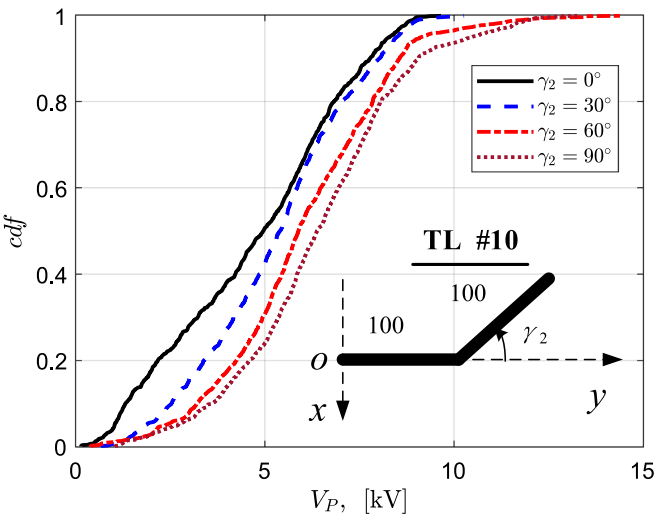

Fig. 6. Cdfs of V_P for power-line network with changing rotation angle γ_2. Terminal: $Z_0 = 50\ \Omega$, $Z_1 = 300\ \Omega$.

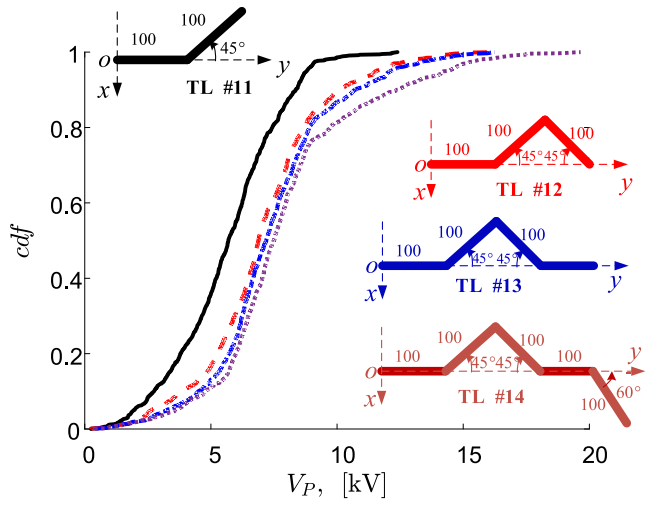

Fig. 7. Cdfs of V_P for power-line network with increased cascaded segments, lengths of all segments are 100 m. $Z_0 = 50\ \Omega$, $Z_1 = 300\ \Omega$.

comprising of 4 segments, then add additional branches at second nodes, generating TL #16 and TL 17. The cdf of V_P is compared in Fig. 8, where one could notice the cdfs are overlapping with each other, despite the branches and complexity of network growing. This result implies that TL branch with the most segments dominating the predictions of overvoltage peak, the role of less-twisted branches can be neglected without leading to noticeable errors. From the viewpoint of network reduction, this property becomes particularly useful for simply a complex TL network, since one can identify the most-twisted branch as the coupling-dominate path for analyzing the worst-case overvoltage peak.

3.1.5. Impact of terminal equipment

In the last example, we consider the impact of far-end terminal equipment, that is, the input impedance modelling power equipment connected to the power line terminals. Without losing generality, the impedances are assumed to be matched to the TL ($Z_1 = Z_C$), overload ($Z_1 < Z_C$) and underloading ($Z_1 > Z_C$), the predicted results are summarized in Fig. 9. It is shown the far-end terminal impedances do have non-negligible impact on V_P, in general large terminal impedance will lead to larger overvoltage peak distribution, this is consistent with common understandings, and imply underloaded even no-load terminal

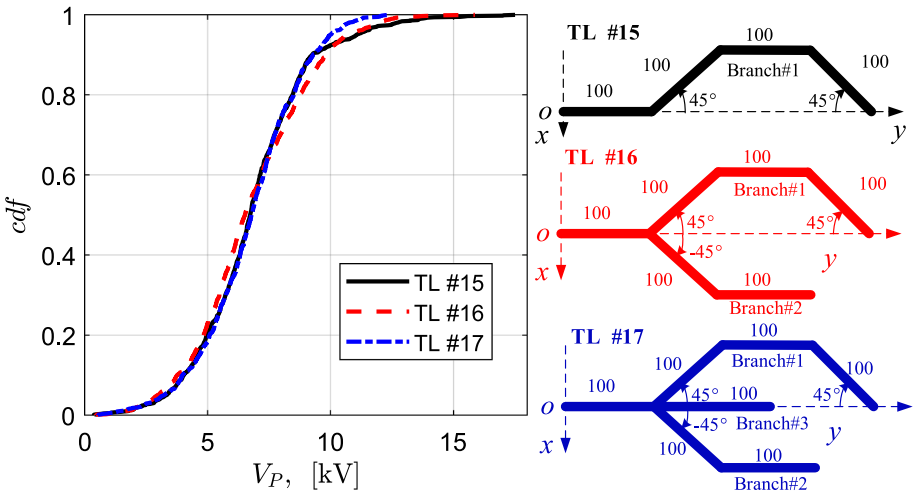

Fig. 8. Cdfs of V_P for power-line network with increasing number of branches, TL #15: $Z_0 = 50\ \Omega$, $Z_1 = 300\ \Omega$; TL #16: $Z_0 = 50\ \Omega$, $Z_1 = 300\ \Omega$, $Z_2 = 200\ \Omega$; TL #17: $Z_0 = 50\ \Omega$, $Z_1 = 300\ \Omega$, $Z_2 = 200\ \Omega$, $Z_3 = 1\ \text{k}\Omega$.

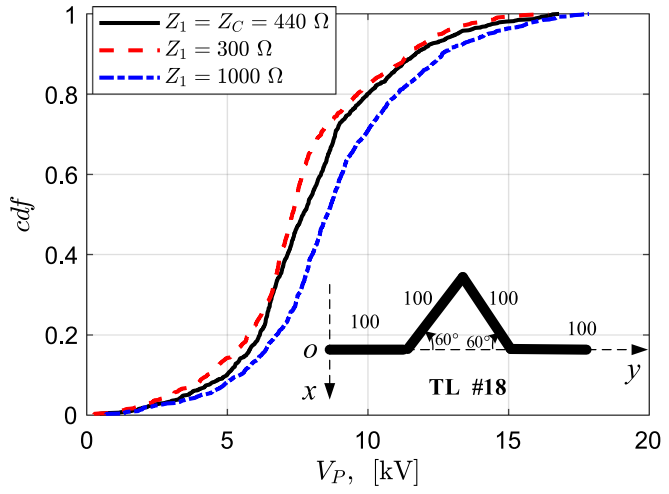

Fig. 9. Cdfs of V_P for power-line network with varying far-end terminal impedance, $Z_0 = 50\ \Omega$.

condition representing a more severe scenario for the proposed analysis.

3.1.6. Power line network reduction

To this end, we could summarize the impacts TL network parameters on the predicted overvoltage peak, simplification strategies can be applied accordingly for network reduction. As shown in Table 1, since it is evident that the cascaded number, orientation and terminal impedance have significant effect on the solution, this information should be fully preserved during the reduction process. Conversely, the branch of most cascaded segment dominates the coupling and can be used to equivalently represent the complex network. The length of individual segments can be flexible adjusted to reduce the complexity of system, since large-scale TL networks are in general difficult to be analyzed, the analysis suggests a small-scale zig-zag branch line is sufficient to approach the original complex TL network for estimating the overvoltage peak.

Table 1
Impact of TL Network Topology on Cdfs of Overvoltage Peak.

Parameter	Impact	Reduction strategy
Orientation	Significant	Unaltered
Length	Negligible	Rescale if necessary
Branch	Reducible	Remove less-twisted branch
Cascaded segment	Significant	Unaltered
Impedance	Significant	Unaltered

3.2. Overvoltage peak upper bound estimation for coupling-dominate branch of power line network

The previous section demonstrates complex TL network could be drastically simplified to the coupling-dominate zigzag branch for analyzing the overvoltage peak. Thus, it is of interest to rigorously formulate the upper bound for a generic zig-zag power line branch.

As shown in Fig. 10, enumerating the zig-zag wire segments from left to right as wire #1, #2, ••••, #n, respectively, where the terminal equipment Z_0 is placed in the origin (O) of Cartesian coordinates. The corresponding segment lengths are $l_1, l_2, \cdots, l_n$, respectively. This power-line network is connected to ground through impedances Z_0 and Z_1 at the left and right terminals, respectively. The rotation angle γ_i of the i^{th} segment is defined as a counterclockwise rotation angle with respect to the $+y$ direction.

3.2.1. Upper bound of overvoltage peak for straight line segment

Considering the simplest case, where a straight line with length l running along y-axis (i.e., power line of only one segment), connected to matched terminal impedances (i.e., $Z_0 = Z_1 = Z_C$), the closed-form expression of $\widehat{L}$ are solved and reported in [27] by a TL model as:

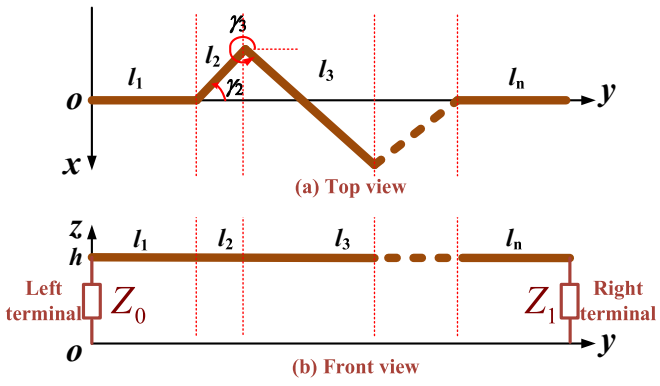

Fig. 10. (a) top view of a zigzag power-line network; (b) front view of the power line, impedances model the terminal power equipment.

$$\widehat{L}(l,\theta,\phi,\gamma) = 2jhG\sin\left(\frac{\beta l}{2}(1+\sin\theta\cos\phi)\right)e^{-j\frac{\beta l}{2}(1+\sin\theta\cos\phi)} \tag{12}$$

$$G(\theta,\phi,\eta) = \frac{\cos\eta(\cos\phi+\sin\theta)+\sin\eta\cos\theta\sin\phi}{1+\sin\theta\cos\phi} \tag{13}$$

where j is the imaginary unit;$\beta = \omega/c_0$ is the phase constant; ω is angular frequency, c_0 is the speed of light in vacuum.

By substituting the coupling efficiency (12) into (9), one obtains the maximal overvoltage for the simplest case of power-line networks (one straight segment) as:

$$V_P = 2h|G|\sqrt{\frac{Z_0W_E}{\pi}\int_{\omega_1}^{\omega_2}\sin^2\left(\frac{\beta l}{2}(1+\sin\theta\cos\phi)\right)d\omega} \tag{14}$$

It can be demonstrated that the long-line saturation property holds for the maximal overvoltage peak V_P, that is, by increasing the length of power line, the value (14) will converge to:

$$\lim_{l\to+\infty} V_P = 2h|G|\sqrt{Z_0W_E(f_2-f_1)} \tag{15}$$

This limit can be approximately reached under the condition $l \gg c_0\pi^{-1}(f_2-f_1)^{-1}(1+\sin\theta\cos\phi)^{-1}$. In view of the large physical scale of power lines, the approximation holds for most realistic systems. This property demonstrates the equivalence between an infinitely long power line and a power line with suitable length in terms of the worst-case field coupling scenario, and could assist the simplification for complex power-line network.

3.2.2. Upper bound of overvoltage peak for Coupling-Dominant Power-line branch

Considering the coupling-dominant power-line branch, which could be modelled by a zig-zag TL line composed by n straight line segments. As shown in Fig. 10. For each segment, the expressions obtained for straight wire (12)-(14) can be readily adapted to address the upper bound of overvoltage peak for oriented TL by substituting ϕ with $\phi-\gamma$, that is, the coupling efficiency of a oriented segment is cast as $\widehat{L}_i^{rot} = \widehat{L}(l_i,\theta_i,\phi_i-\gamma_i,\gamma_i)$.

Consequently, by superimposing all the contributions of the individual segments, the coupling efficiency $\widehat{L}_{NW}$ of whole power-line network can be cast as:

$$\widehat{L}_{NW} = \sum_{i=1}^{n}\widehat{L}_i^{rot}e^{-j\beta\sum_{m=1}^{i-1}l_m[1+\sin\theta\cos(\phi_m-\gamma_m)]} \tag{16}$$

The phase term in (16) accounts for: a) the time delay of the wave propagating from this particular segment's terminal to the power-line network's terminal; b) the phase difference due to reference's origin change in the expressions of the external field. By defining the auxiliary variables $G_i = G(\theta_i,\phi_i-\gamma_i,\gamma_i)$ and τ_i as:

$$\tau_i = \frac{l_i}{c_0}[1+\sin\theta\cos(\phi_i-\gamma_i)] \tag{17}$$

one may simplify (16) as:

$$\widehat{L}_{NW} = 2jh\sum_{i=1}^{n}\sin\left(\frac{\omega\tau_i}{2}\right)e^{-j\frac{\omega\tau_i}{2}}G_ie^{-j\omega\sum_{m=1}^{i-1}\tau_m} \tag{18}$$

Accordingly, the efficiency of field coupling to power-line network with complex routing strategy is finally obtained in the frequency domain. The worst-case analysis for a single straight segment can be applied. Indeed, by substituting in (7) the coupling efficiency $\widehat{L}$ previously stated by (3), the upper bound of overvoltage peak for complex power-line network can be predicted by

$$V_{P,NW} = \sqrt{\frac{Z_0W_E}{\pi}\int_{\omega_1}^{\omega_2}|\widehat{L}_{NW}|^2d\omega} = 2h\sqrt{\frac{Z_0W_E}{\pi}\int_{\omega_1}^{\omega_2}\sum_{i=1}^{n}\sin^2\left(\frac{\omega\tau_i}{2}\right)\left|G_ie^{-j\omega\sum_{m=1}^{i-1}\tau_m}\right|^2d\omega} \tag{19}$$

Although the above *implicit* expression could fulfil the objective of predicting upper bound for field induced overvoltage peak for any power-line network, the contributions due to each segment are complexly coupled through integral and summation, which impedes physical interpretation and offers little information on how to reduce maximal overvoltage from the viewpoint of power system protection. Consequently, the following analysis is devoted to finding an explicit solution by simplifying (19).

Remarkably, likewise in (14) for a single straight line, one can show that each single addend of the summation in (19) becomes independent from length (i.e., from τ_i) if l_i is much greater than a critical electrical length l_s associated to the bandwidth f_2-f_1:

$$l_i \gg l_s = \frac{c_0}{\pi(f_2-f_1)\{1+\sin\theta\cos(\phi_i-\gamma_i)\}} \tag{20}$$

On the other hand, Section 3.1 also suggests that changing the length of any segments exerts negligible effect on the upper bound for the power-line network under analysis, provided that all segments satisfy the "long line" criterium in (20). Accordingly, by flexibly modifying the length of individual segments, an arbitrary large, unique value $\tau = \tau_1 = \tau_2 = \cdots = \tau_n$ can be inconsequentially assigned to (19), which can be rewritten as:

$$V_{P,NW} = 2h\sqrt{\frac{Z_0W_E}{\pi}\int_{\omega_1}^{\omega_2}\sin^2\left(\frac{\omega\tau}{2}\right)\sum_{i=1}^{n}|G_ie^{-j\omega(i-1)\tau}|^2d\omega} \tag{21}$$

In line with the objective of this paper, it is interesting to clearly recognize and separate in (21) the contributions of each single segment. In particular, by imposing the mathematical manipulations reported in Appendix A, a straightforward relation between the maximal overvoltage peak of the power-line network as a whole $V_{P,NW}$ and the one of individual segments $V_{P,i}$ is identified, that is, $V_{P,NW}$ can be simplified as function of $V_{P,i}$:

$$V_{P,NW} = \sqrt{\sum_{i=1}^{n}V_{P,i}^2 - \sum_{i=1}^{n-1}\mathrm{sign}(G_iG_{i+1})V_{P,i}V_{P,i+1}} \tag{22}$$

where signum function sign(x) is defined as:

$$\mathrm{sign}(x) = \begin{cases} 1, & x>0 \\ 0, & x=0 \\ -1, & x<0 \end{cases} \tag{23}$$

It is confirmed that routing strategy playing an important role in the determination of upper bound. In particular, it is worth noting that, in the absence of the second summation in (22), $V_{P,NW}$ could be simply a geometric mean of $V_{P,i}$ pertaining to individual power line segments. Conversely, the second summation implies effects due to adjacent segments (i.e., i^{th} and $(i+1)^{\text{th}}$ segments), that is, effects due to the specific routing geometry.

In the special case when all segments are aligned ($\gamma_i = 0, \forall i$) forming one single straight power line, equation (22) consistently reduces to $V_{P,NT} = V_{P,i}$, that is, to the contribution of just a single segment, which does not depend on length as said above. In general, power line routing, i.e., the presence of unaligned segments may lead to increase/decrease of the overvoltage with respect to a straight line, depending on the relative orientation of adjacent segment according to (22).

3.3. Procedure for evaluating overvoltage peak of complex power line network

To this end, the theory concerning overvoltage peak assessment for a general complex power line network has been discussed in details. A step-by-step flowchart for evaluating the overvoltage peak is presented in Fig. 11, the analysis starts with determining the threat level and power line system scale based on assessment of practical electromagnetic radiation concerns. A generic numerical approach is firstly proposed to predict V_P for arbitrary (topology, terminal) power line network under illumination of arbitrary field (incidence, polarization), the approach exploits the BLT equation for the solution of coupling efficiency in the frequency range of interest.

However, the computation burden of numerical approach grows drastically with the complexity of power line system increasing. To overcome this issue and furthermore, unveiling the coupling mechanism, an analytical solution to the worst-case voltage peak is also formulated, for this purpose, power line network reduction strategy is developed to equivalently represent the complex network to its coupling-dominate zig-zag branch, accordingly, analytical solution based on TL model is obtained, which also reveals the contributions of each segment to the network, the analytical solution can be used to approximate the numerical solution of overvoltage peak, demonstrating a convenient way to assess the worst-case field-coupling response of TL network.

4. Validations and case studies

4.1. Power-line network under case study

In order to verify the existance of the predicted upper bound in (19), a canonical power-line network with routing shown in Fig. 3 is considered. Without losing generality, the proposed exemplification refers to a system composed of 5-segment with radius $r_w = 2.3$ cm and height $h = 4.5$ m, the topology of TL is depicted in the inset of Fig. 12. Assuming the external field excited from direction: $\theta = 73°$, $\phi = 90°$, $\eta = 60°$. An independent TL model exploiting the Baum-Liu-Tesche (BLT) equations [33] was implemented, particularly, without enforcing a priori assumptions related to matched impedances or to the segment lengths. This model is used to directly evaluate the coupling efficiency $\widehat{L}_{NW}$ for matched terminal condition, i.e., $Z_0 = Z_1 = Z_C = 351\ \Omega$, the obtained magnitude $|\widehat{L}_{NW}|$ is reported in Fig. 12.

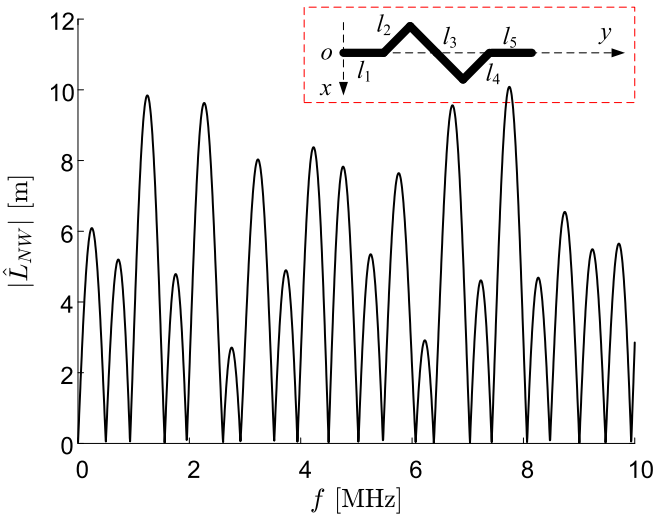

Fig. 12. Coupling efficiency of power line network under analysis (top view of network in the inset). From segment l_1 to l_5, lengths: 100 m, 100 m, 200 m, 100 m, 100 m; orientation angle γ: 0°, 45°, −45°, 45°, 0°.

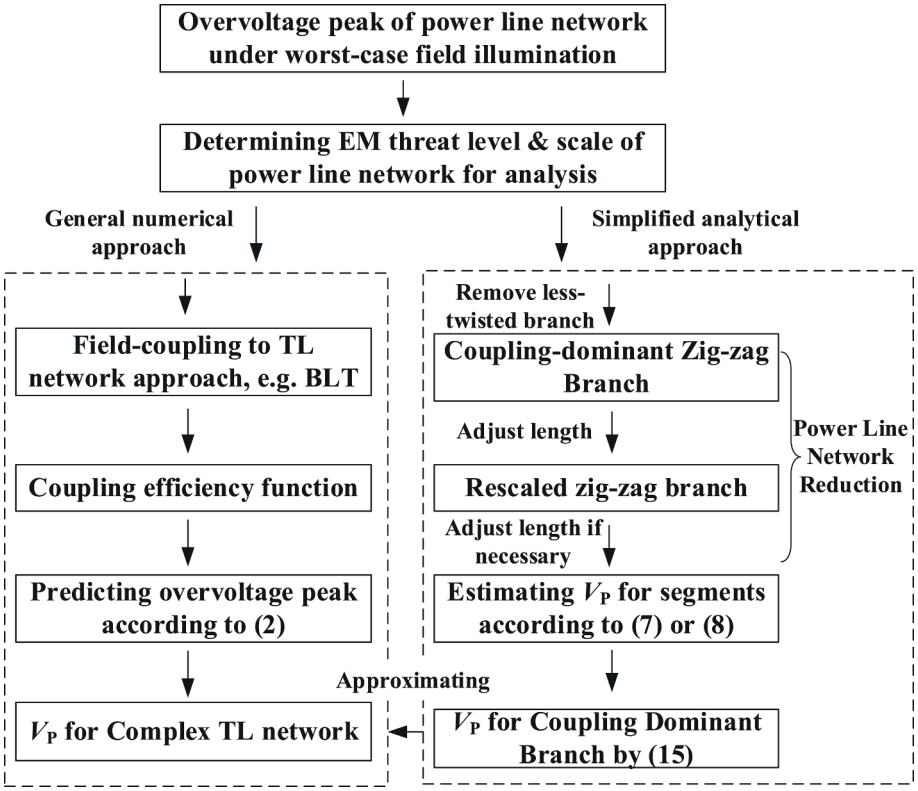

Fig. 11. Step-by-step procedure for evaluating the overvoltage peak for power line system.

4.2. Validation of implicit solution to the upper bound

To verify the proposed upper bound solution, canonical electromagnetic disturbances like Gaussian, double exponential, sinusoid (one cycle) waveforms are considered as comparisons for exciting the system. To enforce the same constraints for consistent comparison, the out-of-band spectra of all fields are filtered out, whereas the amplitudes are conveniently normalized to adjust the energy density to $W_E = 1$ mJ/m^2. The external field and the predicted induced overvoltage waveform in the time-domain are summarized in Fig. 13.

The first row depicted the proposed worst-case disturbance waveform by resorting to (10) and the induced overvoltage waveform, respectively. In the same fashion, the solution for Gaussian, double exponential and sinusoid (one cycle) are reported in the 2nd, 3rd and 4th row, respectively. These canonical electromagnetic disturbances encompass the characteristics of realistic threats to a power system, and the distinct characteristics of the induced overvoltage waveform imply different degree of threat to the system. By assuming correlation between threat level and peak of the overvoltage waveform, one can conclude that the proposed method succeeds in predicting the worst-case scenario, since the induced overvoltage reaches 13.9 kV, whereas the peaks of overvoltage for canonical Gaussian, double exponential and sinusoid fields reach 8.0 kV, 6.3 kV, and 3.1 kV respectively, much smaller than the predicted upper bound.

4.3. Validation of explicit solution to the upper bound

In order to validate the proposed explicit expression (22), consider again the power-line network in Section 4.1. The coupling efficiency evaluated by BLT equations is used to compute the implicit solutions of the upper bound (19) and results are compared versus the proposed explicit solution (22). For greater generality, this is repeated for randomly selected incidence and polarization angles.

As shown in Table 2, the upper bound of overvoltage predicted by explicit solutions are roughly consistent with the implicit solutions. Preciseness depends on the incidence/polarization angles and the maximal relative error (implicit solution as reference) reaches 4.2 % for $\theta = \phi = 30°, \eta = 45°$.Monte Carlo simulations (2000 repeated runs) are performed to evaluate the empirical distribution of the upper bound, with explicit (19) and implicit expression (22) applied as deterministic solutions, respectively, leading to comparison of cumulative distribution

Table 2
Upper Bound of overvoltage predicted by implicit and explicit solution for external field of different directions.

θ	ϕ	γ	Implicit solution, kV	Explicit solution, kV	Relative error, %
90°	70°	0°	15.55	15.50	0.3
45°	70°	90°	14.75	15.16	−2.8
60°	0°	45°	12.04	12.22	−1.5
60°	90°	45°	14.89	14.89	0
30°	30°	45°	15.43	16.08	−4.2
30°	120°	150°	23.08	23.12	−0.2
45°	45°	60°	14.12	14.41	−2.0

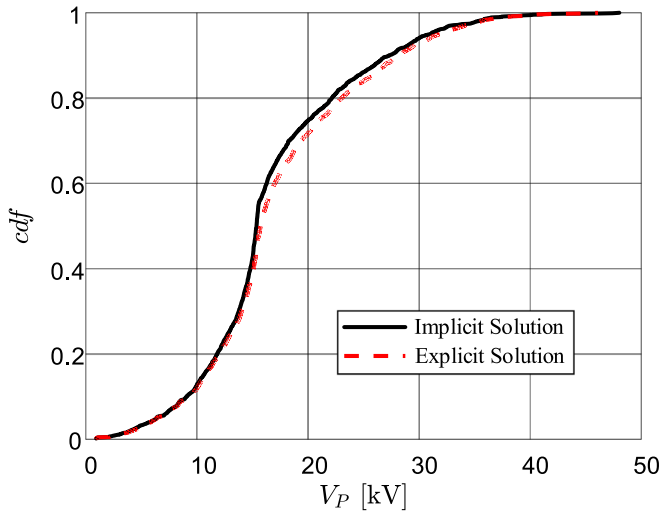

Fig. 14. Cdfs of V_P predicted by explicit solution and implicit solution. The two terminals of network are connected to matched impedances.

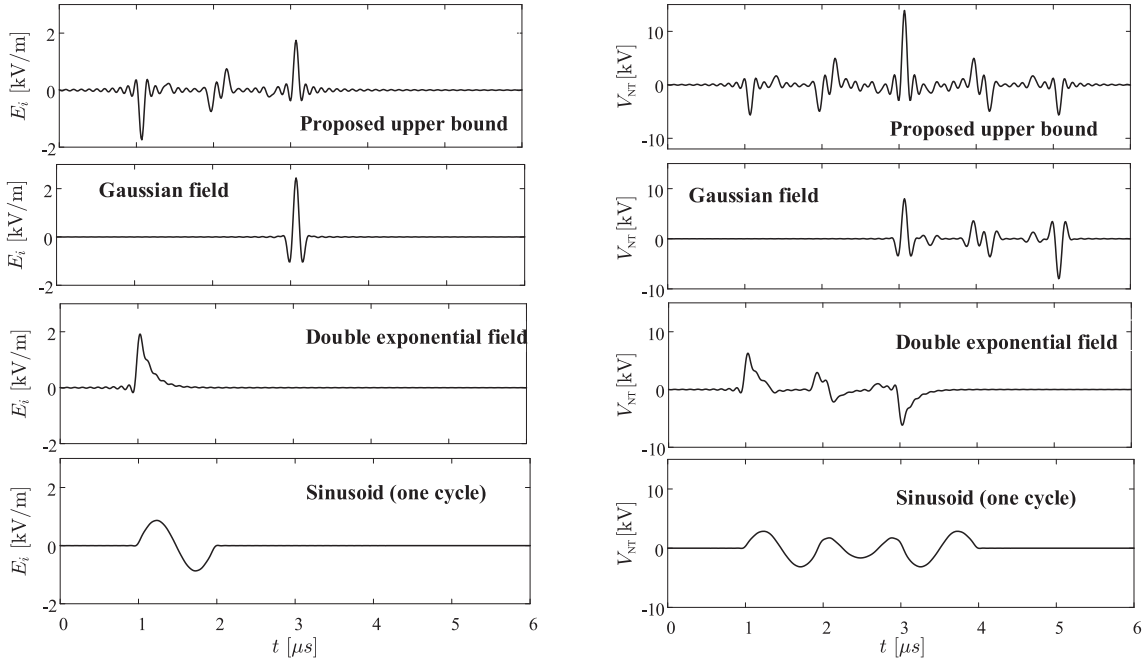

Fig. 13. Comparison of canonical external fields (left column) and induced overvoltage waveforms (right column) for the power-line network under study. The external fields are both filtered and normalized to enforcing both bandwidth and energy density constraint, respectively.

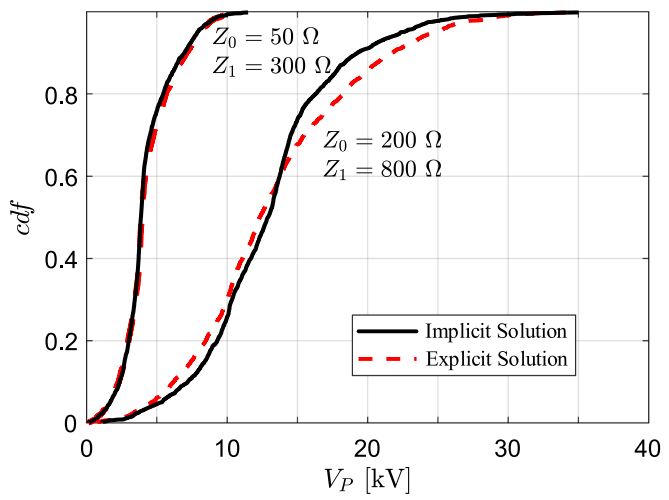

Fig. 15. Cdfs of V_P predicted by explicit solution and implicit solution. The two terminals of network are connected to mismatched impedances.

functions. In the case of matched terminals, the cdfs are compared in Fig. 14, where one can appreciate almost perfect agreement of two distributions; the slight discrepancies could be ascribed to the angles failing to meet (20) for the network under analysis.

4.4. Relaxing the matched terminal assumption

The explicit solution of the upper bound for overvoltage peak is derived under the assumption of matched terminals. For large-scale power systems, the assumption is valid for assessing the overvoltage wave propagation along the long power line. However, if the voltage induced across the power system equipment is of interest, the terminal reflection due to the mismatch between line's characteristic impedance and the input impedance of power system equipment must be included. In this connection, it is interesting to point out that the explicit solution in (22) still roughly valid for mismatched terminals from statistical viewpoint, even though it is rigorously developed for matched terminals.

To prove this statement, in Fig. 15, the cdfs of overvoltage upper bound obtained from both implicit solution and explicit solution are compared for two mismatched cases, i.e., a) the left terminal (at original point) is terminated by $Z_0 = 50\ \Omega$, right terminal is terminated by $Z_1 = 300\ \Omega$; and b) $Z_0 = 200\ \Omega$ and $Z_1 = 800\ \Omega$ are imposed to the two terminals, respectively. Results presented in Fig. 15 suggest that the prediction error of (22) is largely acceptable in the case of mismatching terminals.

5. Conclusions

This paper proposes analytical expressions for predicting the upper bound of overvoltage peaks, which are induced by external electromagnetic disturbances in complex power-line network above lossless ground. Through a rigorous derivation process, based on a TL model of the power line, it is demonstrated that a complex power line system can be equally represented by its coupling-dominate branch for assessing the overvoltage peak from a statistical viewpoint. Accordingly, a power line network reduction strategy is proposed to drastically simplify the system.

Furthermore, it is shown that the upper bound can be assessed by both an implicit solution of the coupling problem as well as an approximated, explicit solution. In particular, the implicit solution highlights the contribution of each power-line section to the overvoltage peak induced in the whole network. It is demonstrated that specific section lengths do not influence the predicted upper bound provided that all the sections are sufficiently long. On the contrary, the routing of the power line, that is, the relative rotation angle between adjacent line sections, can exert a strong impact on the predicted values.

The predicted upper bound turns out to be a useful tool offering a quantitative figure-of-merit for the vulnerability of powerlines with complex layout, under the effects of external electromagnetic disturbances. Possible applications include the design of protection equipment as well as planning of the power line system.

CRediT authorship contribution statement

Tao Liang: Conceptualization, Data curation, Formal analysis, Investigation, Methodology, Validation, Visualization, Writing – original draft, Writing – review & editing. **Giordano Spadacini:** Conceptualization, Methodology, Validation, Writing – original draft, Writing – review & editing. **Sergio A. Pignari:** Supervision, Writing – original draft, Writing – review & editing. **Yan-zhao Xie:** Supervision, Writing – original draft, Writing – review & editing.

Declaration of Competing Interest

The authors declare that they have no known competing financial interests or personal relationships that could have appeared to influence the work reported in this paper.

Data availability

No data was used for the research described in the article.

Acknowledgements

This work was supported by the National Natural Science Foundation of China [52207015].

Appendix A. Derivation of explicit solution to the upper bound for zigzag power line branch

Let variable I denotes the integral term in (21), i.e.,

$$I = \int_{\omega_1}^{\omega_2} \sin^2\left(\frac{\omega\tau}{2}\right) \sum_{i=1}^{n} \left| G_i \mathrm{e}^{-\mathrm{j}\omega(i-1)\tau} \right|^2 d\omega \tag{24}$$

Since the value of $V_{P,NW}$ becomes independent from large value of τ, one can evaluate I by imposing $\tau \to \infty$, that is,

$$I = \lim_{\tau\to\infty} \int_{\omega_1}^{\omega_2} \sin^2\left(\frac{\omega\tau}{2}\right) \sum_{i=1}^{n} \left| G_i \mathrm{e}^{-\mathrm{j}\omega(i-1)\tau} \right|^2 d\omega \tag{25}$$

By separating the real and imaginary parts, the summation term inside the integral can be expanded as

$$\left|\sum_{i=1}^{n} G_i e^{-j\omega(i-1)\tau}\right|^2 = \left|G_1 + G_2 e^{-j\omega\tau} + \cdots + G_n e^{-j(n-1)\omega\tau}\right|^2 \tag{26}$$
$$= |G_1 + G_2\cos(\omega\tau) + \cdots + G_n\cos[(n-1)\omega\tau]|^2 + |G_2\sin(\omega\tau) + \cdots + G_n\sin[(n-1)\omega\tau]|^2$$

By expanding the square operation and combining with trigonometric identity

$$\cos(a)\cos(b) + \sin(a)\sin(b) = \cos(a-b) \tag{27}$$

The summation term can be cast as:

$$\left|\sum_{i=1}^{n} G_i e^{-j\omega(i-1)\tau}\right|^2 = \underbrace{G_1^2 + G_2^2 + \cdots + G_n^2}_{I_1} + \underbrace{2G_1\sum_{i=2}^{n} G_i\cos[(i-1)\omega\tau]}_{I_2} + \underbrace{\sum_{k=2;k>i}^{n}\sum_{i=2}^{n} 2G_iG_k\cos[(i-k)\omega\tau]}_{I_3} \tag{28}$$

By applying the identity $\sin^2(a/2) = (1-\cos a)/2$ to (25), the integrand of I can be fully written as the summation of cosine product. Meanwhile, resorting to Riemann-Lebesgue Lemma [36,37], it is easy to prove:

$$\lim_{\tau\to\infty}\int_{\omega_1}^{\omega_2}\cos(i\omega\tau)\cos(k\omega\tau)d\omega = 0 \tag{29}$$

for unequal integers $i \neq k$.

Therefore, only terms involving the product of same frequency components contribute to the integral. Since $\sin^2(\omega\tau/2)$ contains dc and the 1st order harmonic $\omega\tau$, the effective terms in (28) include only DC terms in I_1, 1st order harmonic terms in I_2 (i.e. $2G_1G_2\cos(\omega\tau)$ when $i = 2$) and in I_3 (i.e.,$2G_2G_3\cos(\omega\tau) + \cdots + 2G_iG_{i+1}\cos(\omega\tau) + \cdots$ when $k = i+1$). Accordingly, I can be dramatically simplified as

$$I = \lim_{\tau\to\infty}\int_{\omega_1}^{\omega_2}\frac{1}{2}\sum_{i=1}^{n} G_i^2 - \sum_{i=1}^{n-1} G_iG_{i+1}\cos^2(\omega\tau)d\omega = \frac{1}{2}\sum_{i=1}^{n} G_i^2 - \frac{1}{2}\sum_{i=1}^{n} G_iG_{i+1} \tag{30}$$

Substituting (30) to (21), the upper bound of overvoltage for power-line network can be obtained for

$$V_{P,NW} = 2h\sqrt{\frac{Z_0W_E}{2\pi}\left(\sum_{i=1}^{n} G_i^2 - \sum_{i=1}^{n} G_iG_{i+1}\right)} \tag{31}$$

In the same fashion, the upper bound of individual segment is given as:

$$V_{P,i} = \lim_{\tau_i\to\infty} 2h\sqrt{\frac{Z_0W_E}{\pi}\int_{\omega_1}^{\omega_2} G_i^2\sin^2(\omega\tau_i)d\omega} = 2h\sqrt{\frac{Z_0W_E}{2\pi}G_i^2} \tag{32}$$

Finally, by combining (31) with (32) and eliminating the variable G_i, one can obtain the explicit solution in (22).

References

[1] Radasky W. Fear of frying electromagnetic weapons threaten our data networks. Here's how to stop them. IEEE Spectr 2014;51:46–51. https://doi.org/10.1109/MSPEC.2014.6882988.

[2] Guo J, Xie Y, Rachidi F. A Semi-Analytical Method to Evaluate Lightning-Induced Overvoltages on Overhead Lines Using the Matrix Pencil Method. IEEE Trans Power Delivery 2018;33:2837–48. https://doi.org/10.1109/TPWRD.2018.2842237.

[3] Szewczyk M, Kuniewski M, Piasecki W, Florkowski M, Straumann U. Determination of Breakdown Voltage Characteristics of 1'100 kV Disconnector for Modelling of VFTO in Gas-Insulated Switchgear. IEEE Trans Power Delivery 2016;31:2151–8. https://doi.org/10.1109/TPWRD.2015.2513080.

[4] Sekioka S, Otoguro H, Funabashi T. A Study on Overvoltages in Windfarm Caused by Direct Lightning Stroke. IEEE Trans Power Delivery 2019;34:671–9. https://doi.org/10.1109/TPWRD.2018.2883910.

[5] Miyazaki T, Okabe S, Sekioka S. An Experimental Validation of Lightning Performance in Distribution Lines. IEEE Trans Power Delivery 2008;23:2182–90. https://doi.org/10.1109/TPWRD.2008.919252.

[6] Rakov VA, Uman MA, Fernandez MI, Mata CT, Rambo KJ, Stapleton MV, et al. Direct lightning strikes to the lightning protective system of a residential building: triggered-lightning experiments. IEEE Trans Power Delivery 2002;17:575–86. https://doi.org/10.1109/61.997942.

[7] Szewczyk M, Pawłowski J, Kutorasiński K, Piasecki W, Florkowski M, Straumann U. High-Frequency Model of Magnetic Rings for Simulation of VFTO Damping in Gas-Insulated Switchgear With Full-Scale Validation. IEEE Trans Power Delivery 2015;30:2331–8. https://doi.org/10.1109/TPWRD.2015.2417675.

[8] Andreotti A, Assante D, Mottola F, Verolino L. An exact closed-form solution for lightning-induced overvoltages calculations. IEEE Trans Power Delivery 2009;24:1328–43. https://doi.org/10.1109/TPWRD.2008.2005395.

[9] Piantini A. Extension of the Rusck model for calculating lightning-induced voltages on overhead lines considering the soil electrical parameters. IEEE Trans Electromagn Compat 2016;59:154–62. https://doi.org/10.1109/TEMC.2016.2601011.

[10] Rachidi F, Nucci CA, Ianoz M, Mazzetti C. Influence of a lossy ground on lightning-induced voltages on overhead lines. IEEE Trans Electromagn Compat 1996;38:250–64. https://doi.org/10.1109/15.536054.

[11] Nucci CA, Rachidi F, Ianoz MV, Mazzetti C. Lightning-induced voltages on overhead lines. IEEE Trans Electromagn Compat 1993;35:75–86. https://doi.org/10.1109/15.249398.

[12] De Conti A, Leal OE. Time-domain procedures for lightning-induced voltage calculation in electromagnetic transient simulators. IEEE Trans Power Delivery 2020;36:397–405. https://doi.org/10.1109/TPWRD.2020.2982306.

[13] Yokoyama S, Miyake K, Fuki S. Advanced observations of lightning induced voltage on power distribution lines. II IEEE Trans Power Delivery 1989;4:2196–203. https://doi.org/10.1109/61.35647.

[14] De Conti A, Perez E, Soto E, Silveira FH, Visacro S, Torres H. Calculation of lightning-induced voltages on overhead distribution lines including insulation breakdown. IEEE Trans Power Delivery 2010;25:3078–84. https://doi.org/10.1109/TPWRD.2010.2059050.

[15] Borghetti A, Nucci CA, Paolone M. An Improved Procedure for the Assessment of Overhead Line Indirect Lightning Performance and Its Comparison with the IEEE Std. 1410 Method. IEEE Trans Power Delivery 2007;22:684–92. https://doi.org/10.1109/TPWRD.2006.881463.

[16] Chen J, Zhu M. Calculation of Lightning Flashover Rates of Overhead Distribution Lines Considering Direct and Indirect Strokes. IEEE Trans Electromagn Compat 2014;56:668–74. https://doi.org/10.1109/TEMC.2014.2309146.

[17] Rachidi F. A review of field-to-transmission line coupling models with special emphasis to lightning-induced voltages on overhead lines. IEEE Trans Electromagn Compat 2012;54:898–911. https://doi.org/10.1109/TEMC.2011.2181519.

[18] Liu M-Z, Xie Y-Z, Chen Y-H, Liu Q. Modelling the 10,000-Year Geomagnetic Disturbance Scenarios Based on Extreme Value Analysis. IEEE Lett Electromag Compat Pract Appl 2020;2:156–60. https://doi.org/10.1109/LEMCPA.2020.3042457.

[19] Liu Q, Xie Y, Dong N, Chen Y, Liu M, Li Q. Uncertainty Quantification of Geo-Magnetically Induced Currents in UHV Power Grid. IEEE Trans Electromagn Compat 2020;62:258–65. https://doi.org/10.1109/TEMC.2019.2894945.

[20] Nazir M, Burkes K, Enslin JH. Converter-Based Solutions: Opening New Avenues of Power System Protection Against Solar and HEMP MHD-E3 GIC. IEEE Trans Power Delivery 2021;36:2542–9. https://doi.org/10.1109/TPWRD.2020.3016207.

[21] Li F, Liu Y, Tarditi AG, Li Z. Simulation of Fast-Rise Transients in a Large-Power Transformer Winding. IEEE Trans Electromagn Compat 2020;62:478–88. https://doi.org/10.1109/TEMC.2019.2909280.
[22] Kruse VJ, Tesche FM, Liu TK, Barnes PR. Flashover vulnerability of transmission and distribution lines to high-altitude electromagnetic pulse (HEMP). IEEE Trans Power Delivery 1990;5:1164–9. https://doi.org/10.1109/61.53136.
[23] Laour M, Tahmi R, Vollaire C. Experimental evaluation and FDTD method for predicting electromagnetic fields in the near zone radiated by power converter systems. Turk J Electr Eng Comput Sci 2017;25:1460–71.
[24] Ge Y, Xie Y, Liang T, Dong N, Wu Y, Wang Y, et al. A Test Method for Response Behavior of Metal-Oxide Arrester Subjected to Transient Electromagnetic Disturbances. IEEE Transactions on Power Delivery 2022:1–1. https://doi.org/10.1109/TPWRD.2022.3157994.
[25] Spadacini G, Liang T, Grassi F, Pignari SA. Worst Case and Statistics of Waveforms Involved in Wideband Intentional Electromagnetic Attacks. IEEE Trans Electromagn Compat 2018;60:1436–44. https://doi.org/10.1109/TEMC.2017.2778017.
[26] Liang T, Spadacini G, Grassi F, Pignari SA. Worst-Case Wideband Radiated IEMI for Unshielded and Shielded Cables: A Statistical Analysis of the Main Influencing Parameters. IEEE Trans Electromagn Compat 2019;61:1244–52. https://doi.org/10.1109/TEMC.2019.2909824.
[27] Liang T, Spadacini G, Grassi F, Pignari SA. Coupling of wideband radiated IEMI to cables above ground. IEEE Trans Electromagn Compat 2018;62:589–97. https://doi.org/10.1109/TEMC.2018.2877508.
[28] Tesche FM. Development and Use of the BLT Equation in the Time Domain Development and Use of the BLT Equation in the Time Domain. IEEE Trans Electromagn Compat 2006;49:3–11. https://doi.org/10.1109/Temc.2007.888184.
[29] Tesche FM, Ianoz M, Karlsson T. EMC analysis methods and computational models. John Wiley & Sons; 1997.
[30] Leone M, Singer HL. On the coupling of an external electromagnetic field to a printed circuit board trace. IEEE Trans Electromagn Compat 1999;41:418–24. https://doi.org/10.1109/15.809842.
[31] Agrawal AK, Price HJ, Gurbaxani SH. Transient response of multiconductor transmission lines excited by a nonuniform electromagnetic field. IEEE Transactions on Electromagnetic Compatibility 1980;EMC-22:119–29. https://doi.org/10.1109/TEMC.1980.303824.
[32] Cooray V. Calculating lightning-induced overvoltages in power lines. A comparison of two coupling models. IEEE Trans Electromagn Compat 1994;36:179–82. https://doi.org/10.1109/15.305462.
[33] Paul CR. Analysis of multiconductor transmission lines. New York: IEEE; 2007. https://doi.org/10.1109/9780470547212.
[34] Prather WD, Baum CE, Torres RJ, Sabath F, Nitsch D. Survey of Worldwide High-Power Wideband Capabilities. IEEE Trans Electromagn Compat 2004;46:335–44. https://doi.org/10.1109/TEMC.2004.831826.
[35] Napolitano F. An Analytical Formulation of the Electromagnetic Field Generated by Lightning Return Strokes. IEEE Trans Electromagn Compat 2011;53:108–13. https://doi.org/10.1109/TEMC.2010.2065810.
[36] Kahane CS. Generalizations of the Riemann-Lebesgue and Cantor-Lebesgue lemmas. Czechoslov Math J 1980;30:108–17.
[37] Torres M. Several Aspects Around the Riemann-Lebesgue Lemma. J Adv Res Pure Math 2013;5:33–46. https://doi.org/10.5373/jarpm.1458.052712.